Supplemental Information for:

Adsorption and photocatalytic desorption toward Cr(VI) over defect-induced hierarchically porous UiO-66-$(OH)_2$: A sustainable approach

Yu-Hang Li[1, 2], Meng-Yuan Liu[1, 2], Yu-Wei Wei[1, 2], Chong-Chen Wang[1, 2,*], Peng Wang[1, 2]

[1] Beijing Key Laboratory of Functional Materials for Building Structure and Environment Remediation, School of Environment and Energy Engineering, Beijing University of Civil Engineering and Architecture, Beijing 100044, China.

[2] Beijing Energy Conservation & Sustainable Urban and Rural Development Provincial and Ministry Co-construction Collaboration Innovation Center, Beijing University of Civil Engineering and Architecture, Beijing 100044, China.

Number of Pages: 24

Number of Text Sections: 6

Number of Tables: 6

Number of Figures: 11

*Corresponding author.

E-mail address: wangchongchen@bucea.edu.cn, chongchenwang@126.com (C.-C. Wang).

Section S1. Chemicals

Zirconium (IV) chloride ($ZrCl_4$, purity ≥ 99 %), 2,5-Dihydroxyterephthalic acid ($H_2BDC-(OH)_2$, purity ≥ 98 %) ammonium metavanadate (NH_4VO_3, purity ≥ 99 %) and potassium perrhenate ($KReO_4$, purity ≥ 98 %) were brought from J&K company. benzoic acid (BA, purity ≥ 99 %) was purchased from MACKUIN company. Dimethylformamide (DMF), hydrochloric acid (HCl), methanol (MeOH), acetic acid (purity ≥ 99.5 %) were obtained from Tianjin Fu Chen Chemical Co., Ltd. (China). Sodium arsenite ($NaAsO_2$, purity ≥ 90 %) was brought from ALDRICH Chemistry Co., Ltd. (China). Potassium dichromate ($K_2Cr_2O_7$, analytically pure) was brought from Beijing Chemical Reagent Co., Ltd. (China). All chemicals were directly used without further purification.

Section S2. Characterizations

The powder X-ray diffraction (PXRD) patterns were obtained on a DX-2700B X-ray diffractometer using Cu Kα radiation. Fourier transform infrared spectra (FTIR) were measured by a Nicolet 6700 infrared spectrophotometer with KBr pellets. The thermogravimetric analyses-differential scanning calorimetry (TGA-DSC) was measured by Mettler-Toledo TGA/DSC 3+ and Elementar Vario EL cube, respectively. The surface area and pore size distribution were obtained on a micromeritics ASAP 2460 at 77 K adopting the Brunauer-Emmett-Teller (BET) method. The scanning electron microscope (SEM) and high-resolution transmission electron microscope (HR-TEM) were acquired by SU8020, JEM 1200EX and Tecnai G2 F20, respectively. Photoluminescence (PL) emission spectra were tested on Hitachi F-7000 spectrophotometer in the range of 300-600 nm a at room temperature with an excitation wavelength of 369 nm. High-resolution X-ray photoelectron spectra (XPS) measurement was

performed on a Thermo ESCALAB 250XI. UV-Vis diffuse reflectance spectra (UV-Vis DRS) were tested on a PerkinElmer Lambda 650S spectrophotometer with BaSO4 as the reference.

Section S3. UiO-66-$(OH)_2$ Synthesis

UiO-66-$(OH)_2$ was synthesized according to a reported with a minor modification. Particularly, the solutions of 0.1716 mmol $ZrCl_4$ (40.0 mg) and 0.1716 mmol ligand (2,5-Dihydroxyterephthalic acid (33.99 mg)) dissolved in 10.0 mL N,N-dimethylformamide (DMF). Then, 3.0 mL acetic acid was added to the mixed solution. The mixed solution was transferred into a 25.0 mL Teflon lined autoclave, followed by heating at 120 ℃ for 24 h. Then, the generated powder was washed with methyl alcohol four times and dried at 60 ℃ for 12 h.

Section S4. Batch adsorption experiments

The Cr(VI) adsorption experiments were performed by using $K_2Cr_2O_7$ as the model pollution. H_2SO_4 or NaOH solution with appropriate concentration were using to adjust the required pH values of solution. During the sorption process, each 2.0 mL suspension liquid was filtered via using 0.45 μm PTFE membrane at specified time intervals. The adsorption capacity (q_e) of adsorbent was calculated by Eq. S1:

$$q_e = \frac{(C_0 - C_e)V}{M} \quad \text{(S1)}$$

Where, q_e (mg g^{-1}) was the sorption capacity, C_0 and C_e (mg L^{-1}) represented the initial and equilibrium concentration of Cr(VI), respectively.

As to sorption kinetic experiments, the fresh adsorbent (20.0 mg) was added into the 150.0 mL 30.0 mg L^{-1} Cr(VI) solution. Then, the mixed solution was shaken in the constant temperature shaker (HNY-2102C) with the speed of 170 rpm until 240.0 min to reach adsorption-desorption equilibrium at 298 K and pH = 2.0. The pseudo-first-order, pseudo-second-order and

Weber-Morris intraparticle diffusion models were selected to fit the kinetic curves, respectively (SI, Section S5). For sorption isotherms and thermodynamic parameters, the sorption experiments of optimal adsorbent were performed under 288 K, 298 K and 308 K with identical condition. The Langmuir, Freundlich and Dubinin-Radushkevich (D-R) models were used to fit the isotherm curves, respectively (SI, Section S5).

Section S5. Data Analysis

Analysis of Adsorption Kinetic Data.

The curves were fitted by using pseudo-first-order model (Eq. S2), pseudo-second-order model (Eq. S3) and Weber-Morris intra-particle diffusion model (Eq. S4).

$$\ln\left(q_e - q_t\right) = \ln\left(q_t\right) - k_1 t \quad \text{(S2)}$$

$$t/q_t = 1/(k_2 \times q_e^2) + t/q_e \quad \text{(S3)}$$

$$q_t = kt^{0.5} + C \quad \text{(S4)}$$

where q_e and q_t (mg g^{-1}) were the adsorption capacity at equilibrium and a specific time, respectively. k_1, k_2 (min^{-1}) and k (mg g^{-1} min$^{0.5}$) respectively represented the rate constant of pseudo-first-order model, pseudo-second-order model, and Weber-Morris models.

Analysis of Adsorption Isotherms Data.

The adsorption isotherms were fitted using the Langmuir model (Eq. S5), Freundlich model (Eq. S6) and Dubinin-Radushkevich (D-R) model (Eqs. S7, S8 and S9):

$$C_e/q_e = 1/(K_L \times q_m) + C_e/q_m \quad \text{(S5)}$$

$$\ln q_e = \ln K_f + (1/n)\ln C_e \quad \text{(S6)}$$

$$\ln q_e = \ln q_m - K_{DR}\xi^2 \quad \text{(S7)}$$

$$\xi = RT\ln\left(1 + (1/C_e)\right) \quad \text{(S8)}$$

$$E = 1/(2 \times K_{DR})^{0.5} \quad \text{(S9)}$$

where C_e (mg L^{-1}) was the remaining concentration of Pb(II) at equilibrium. K_L, K_f $K_{D\text{-}R}$ and n respectively represented the constant of different models, ξ (J mol^{-1}) and E (kJ mol^{-1}) respectively represented polar potential energy and adsorption free energy.

Calculation of Thermodynamic Parameters.

All the thermodynamic parameters like ΔG^0 (the standard free energy change), ΔH^0 (enthalpy change) and ΔS^0 (entropy change) were calculated via Eqs. S10 and S11:

$$\ln K_d = \frac{\Delta S^0}{R} - \frac{\Delta H^0}{RT} \quad \text{(S10)}$$

$$\Delta G^0 = \Delta H^0 - T\Delta S^0 \quad \text{(S11)}$$

where R (8.314 kJ mol^{-1} K^{-1}) represented the gas constant and T (K) represented the temperature.

Distribution coefficient K_d (mL g^{-1}), which is mass-weighted partition coefficient between solid phase and liquid supernatant phase reflecting the selectivity for objective metal ions, was calculated according to the formula:

$$K_d = \frac{C_0 - C_e}{C_e} \times \frac{V}{M} \quad \text{(S12)}$$

where, C_0 and C_e (mg L^{-1}) were the concentrations of Cr(VI) at contact time of initial concentration and final concentration, V (mL) is the volume of Cr(VI) solution and M (g) is the mass of adsorbent.

Section S6. TGA analysis.

Considering the TGA tests were run up to 800 ℃ under air atmosphere at a heating rate of 10 ℃/min. These conditions can ensure the residue of every TGA experiment is ZrO_2. In this

case, the reaction equation for the complete combustion of ideal UiO-66-$(OH)_2$: Zr_6O_6(BDC-$(OH)_2)_6$:

$$Zr_6O_6(BDC - (OH)_2)_6(s) + 56O_2 \xrightarrow{\Delta} 6ZrO_2 + 48CO_2(g) + 6NH_3(g) + 10H_2O(g)$$

The molar mass of Zr_6O_6(BDC-$(OH)_2)_6$ was 1833.56 g mol^{-1}, which was 2.48 times higher than the solid residue 6.0 mol of ZrO_2 (6×123.22 = 739.34 g mol^{-1}). Thus, if the end weight (the mass at 800 ℃) of a TGA run on UiO-66-$(OH)_2$ was normalized to 100 %, the TGA plateau of ideal UiO-66-$(OH)_2$ (dehydroxylated UiO-66-$(OH)_2$, Zr_6O_6(BDC-$(OH)_2)_6$) should be found at 248% on the TGA trace. However, it usually fell short than that of the theoretical weight, indicating that the as-prepared UiO-66-$(OH)_2$ framework was lighter than that formulated in the idealized equation. This finding suggested that the UiO-66-$(OH)_2$ sample may be linker deficient. It was important to note that the ratio of BDC-$(OH)_2$: Zr obtained from TGA represented the mean coordination number, which cannot distinguish missing linker and missing cluster defects. The number of linker deficiencies per Zr_6 formula unit (x) was calculated by the following (Eqs. S13, S14 and S15):

$$Wt.PL_{Pre} = \frac{(W_{Pre} - W_{End})}{NL_{Pre}} \quad \text{(S13)}$$

$$NL_{Exp} = (6 - x) = \frac{(W_{Exp} - W_{End})}{W_t.PL_{Pre}} \quad \text{(S14)}$$

$$x = 6 - NL_{Exp} \quad \text{(S15)}$$

where: W_{End} was the end weight of the TGA trace (normalized to 100%), W_{Pre} was the theoretical weight of the dehydroxylated UiO-66-$(OH)_2$ (Zr_6O_6(BDC-$(OH)_2)_6$: 1833.56 g/mol), $W_t.PL_{pre.}$ was a value for the theoretical weight loss per BDC-$(OH)_2$ linker, 6 was the number of linkers in the ideal Zr-oxo unit, W_{Exp} was the corresponding experimental value, and $NL_{Exp.}$ was

the number of BDC-$(OH)_2$ linker in experiment.

Table S1. The kinetic models fitting parameters of UiO-66, UiO-66-$(OH)_2$ and series HP-UOH-*X* toward Cr(VI) adsorption.

Adsorbents	Pseudo-first-order model			Pseudo-second-order model			Measured value
	q_{e1}	k_1	R^2	q_{e2}	k_2	R^2	
UiO-66	4.34	0.017	0.632	17.96	1.7×10^{-2}	0.999	17.83
UiO-66-$(OH)_2$	67.53	0.013	0.995	89.85	1.8×10^{-4}	0.993	73.22
HP-UOH-20	114.29	0.015	0.995	148.15	1.3×10^{-4}	0.998	122.11
HP-UOH-40	118.81	0.013	0.981	164.74	1.5×10^{-4}	0.997	145.09
HP-UOH-80	131.27	0.015	0.984	182.15	1.6×10^{-4}	0.999	161.76
HP-UOH-160	127.42	0.013	0.996	167.78	1.1×10^{-4}	0.999	140.62

Postscript:

q_{e1}, q_{e2}: mg g^{-1}, k_2: g·mg^{-1} min^{-1}, k_1: min^{-1}.

Table S2. The Weber-Morris model fitting parameters of UiO-66, UiO-66-$(OH)_2$ and various HP-UOH-*X* towards Cr(VI) adsorption.

Adsorbents	Weber-Morris model					
	k_1	R^2	k_2	R^2	k_3	R^2
UiO-66	1.57	1.000	–	–	0.07	0.832
UiO-66-$(OH)_2$	5.45	0.997	4.24	0.996	3.14	1.000
HP-UOH-20	9.33	0.997	4.52	0.974	–	–
HP-UOH-40	12.33	0.997	6.01	0.999	–	–
HP-UOH-80	14.21	0.998	6.25	0.997	–	–
HP-UOH-160	10.01	0.998	5.73	0.999	–	–

Postscript:

k_1, k_2, k_3: mg g^{-1} $min^{0.5}$.

Table S3. Constants of isotherm models of HP-UOH-80 towards Cr(VI) adsorption at various temperatures.

T (K)	Langmuir model			Freundlich model			D-R model		
	K_L	q_m	R^2	K_f	$1/n$	R^2	K_{DR}	E	R^2
288	0.164	159.23	0.995	50.41	0.278	0.996	2.38×10^{-6}	458.35	0.844
298	0.217	226.24	0.986	69.50	0.303	0.999	4.45×10^{-7}	1059.99	0.774
308	0.348	284.9	0.978	92.27	0.319	0.996	7.85×10^{-8}	2523.77	0.696

Postscript:

q_m: mg g^{-1}, K_L: L mg^{-1}, K_f: L g^{-1}, E: kJ mol^{-1}.

Table S4. Thermodynamic parameters of the adsorption behavior over HP-UOH-80 towards Cr(VI) adsorption at different temperatures.

T (K)	K_d	ΔG^o	ΔS^o	ΔH^o
288	3230.71	-19.31		
298	5314.77	-21.33	201.96	38.85
308	9276.19	-23.35		

Postscript:

K_d: mL g^{-1}, ΔG^o: kJ mol^{-1}, ΔS^o: J mol^{-1} K^{-1}, ΔH^o: kJ mol^{-1}.

Table S5. The concentration of different inorganic anions and organic matters.

Parameters	Cl^-	NO_3^-	HCO_3^-	SO_4^{2-}	$H_2PO_4^-$	HA
Concentration (mg L^{-1})	98.25	9.25	206	100.25	2.65	5.0

Note: The concentration of the five above-stated factors based on the characteristics of surface water quality in some areas of Beijing.

Table S6. Characteristics of tap water and lake water used for Cr(VI) removal by HP-UOH-80.

Parameters	Tap water	Lake water
pH	2.0	2.0
Na^{+} (mg L^{-1})	10.69	37.1
K^{+} (mg L^{-1})	1.856	4.4
Mg^{2+} (mg L^{-1})	11.64	33.3
Ca^{2+} (mg L^{-1})	47.79	69.8
SO_4^{2-} (mg L^{-1})	7.47	175.1
Cl^{-} (mg L^{-1})	17.9	32.2
NO_3^{-} (mg L^{-1})	26.6	10.8
F^{-} (mg L^{-1})	0.182	NA
PO_4^{3-} (mg L^{-1})	NA	0.38

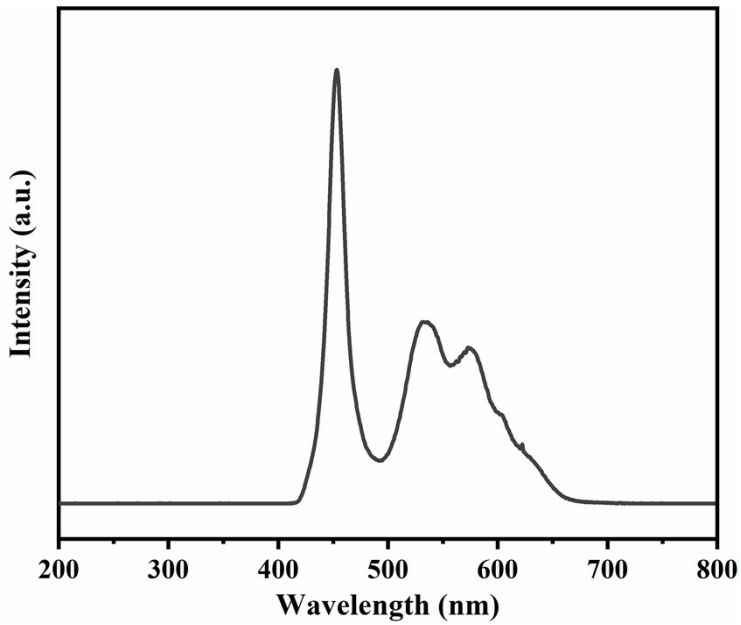

Fig S1 The spectrum of visible light source.

Fig. S2 The setup picture of the fixed-bed column experiments.

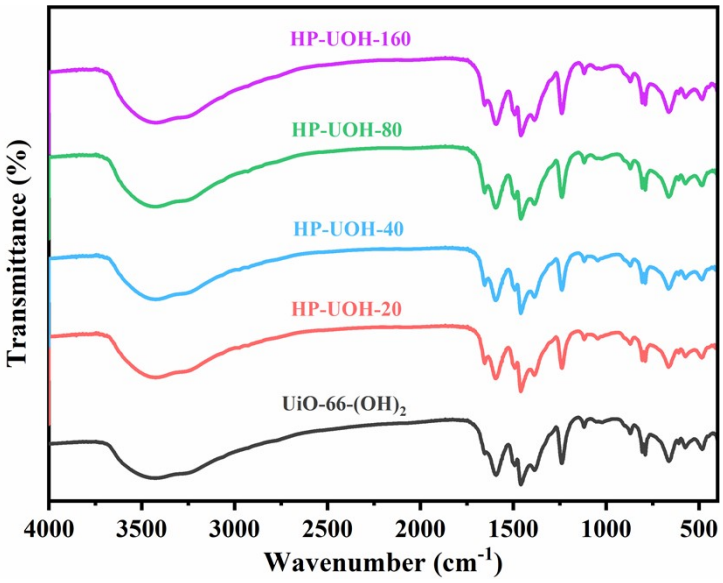

Fig. S3 FTIR spectra of UiO-66-$(OH)_2$ and various HP-UOH-*X* samples.

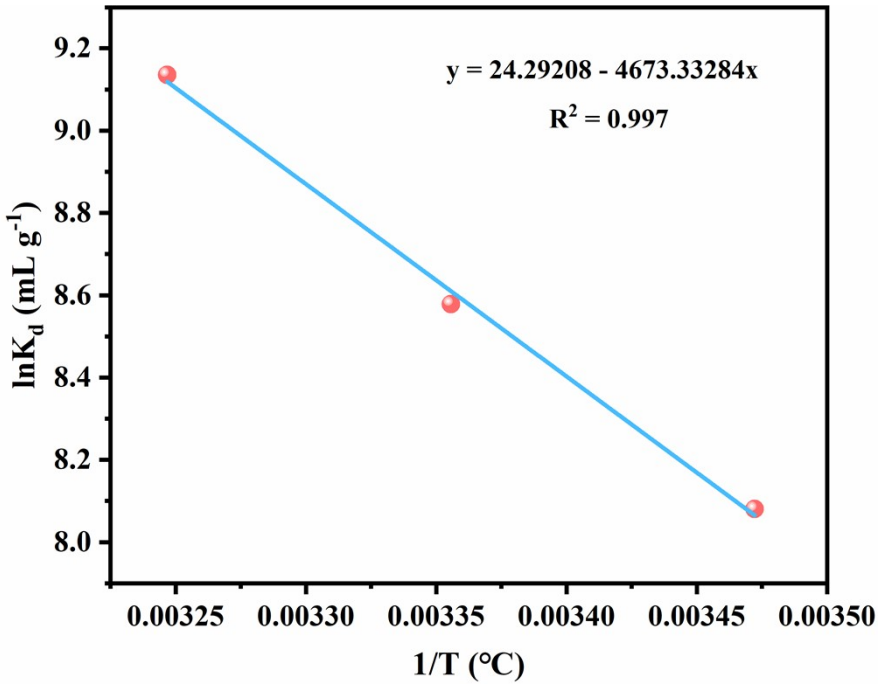

Fig. S4 The straight line obtained from plotting $\ln K_d$ versus 1/T.

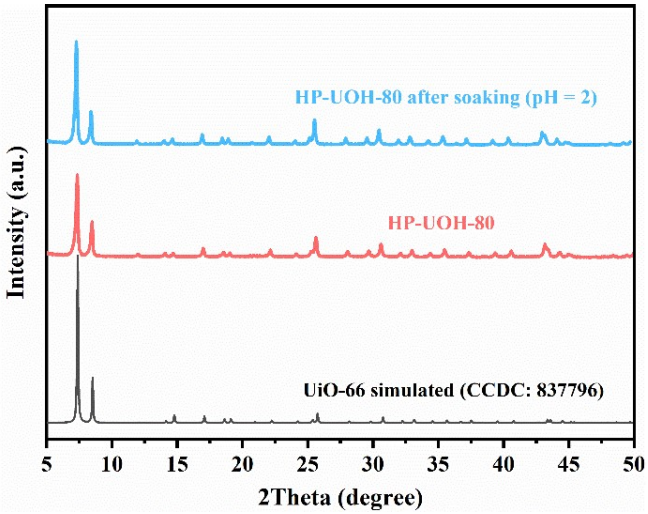

Fig. S5 The PXRD patterns of pristine HP-UOH-80 and HP-UOH-80 after soaking by acidic solution.

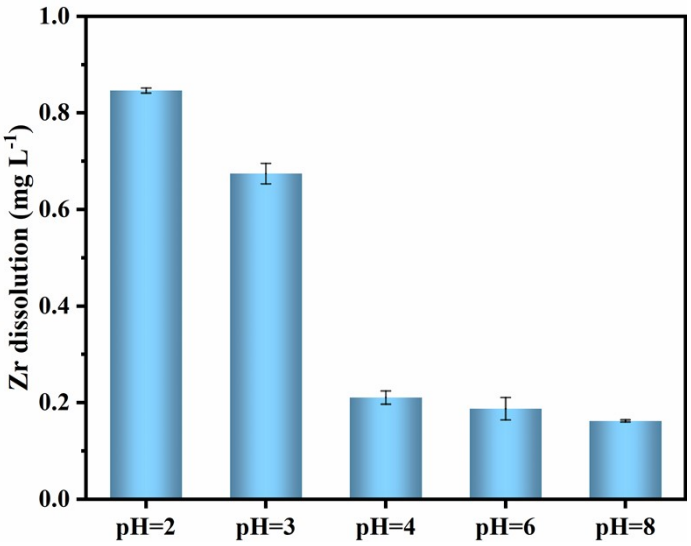

Fig. S6 The Zr dissolution of HP-UOH-80 in aqueous solution with different initial pH values.

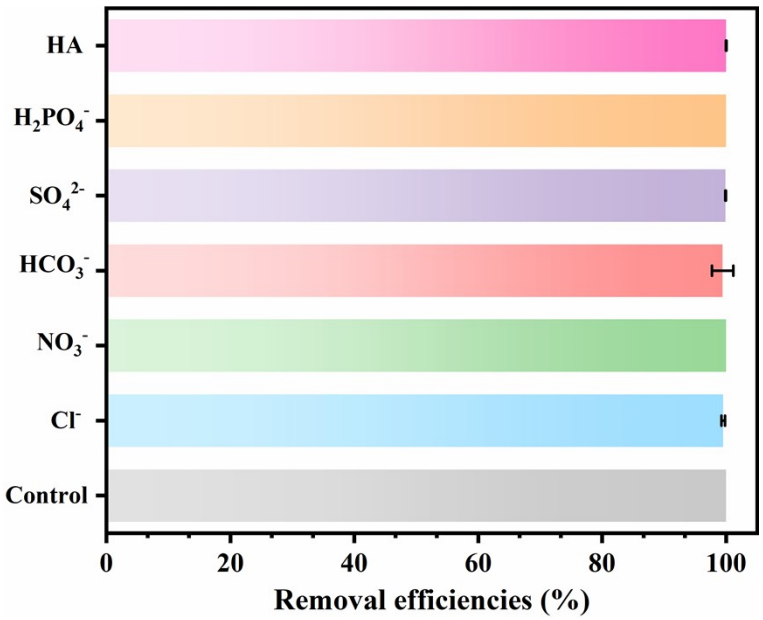

Fig. S7 The influence of co-existing inorganic ions and organic matters on Cr(VI) removal efficiencies.

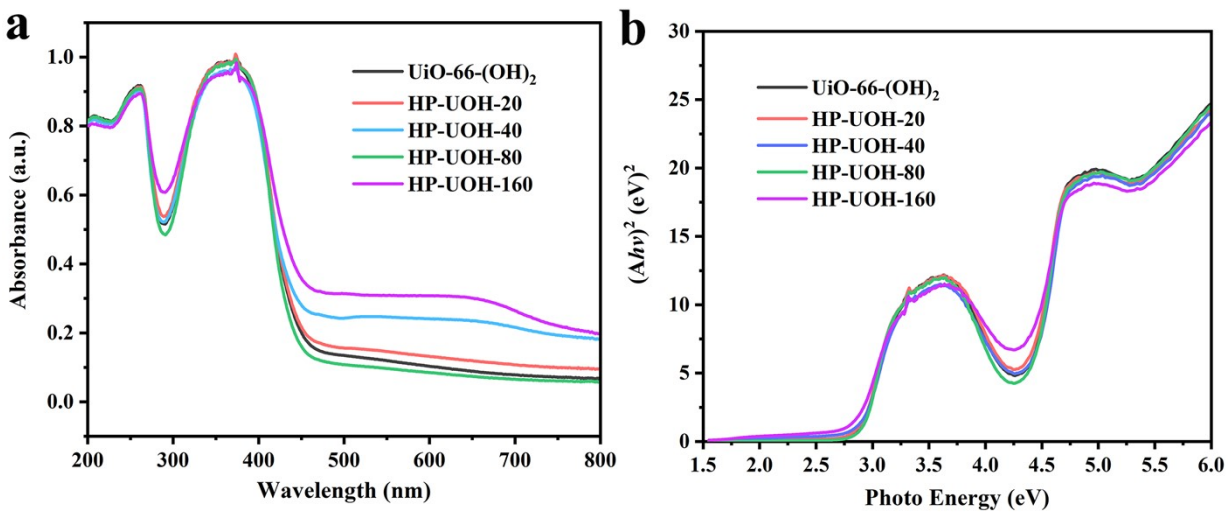

Fig. S8 (a) The UV-vis DRS spectra and (b) the E_g plots of UiO-66-$(OH)_2$ and series HP-UOH-*X*.

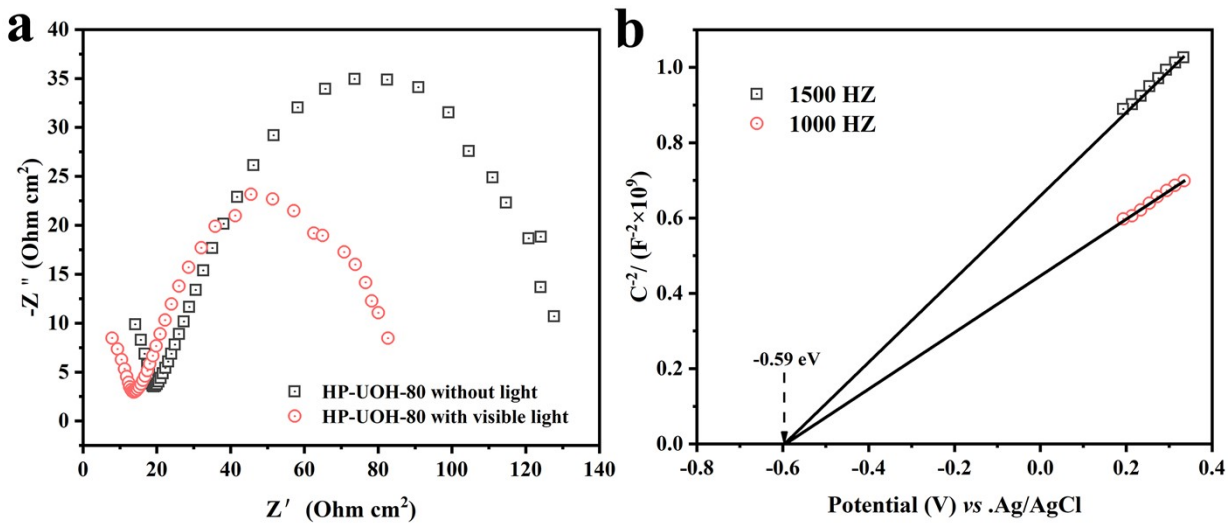

Fig. S9 The (a) EIS analysis and (b) Mott-Schottky curves at different frequencies of HP-UOH-80.

Note: because the flat band potential was more positive 0.1 eV than the conduction band potential for n-typed semiconductor [1], the E_{LUMO} of HP-UOH-80 was calculated as −0.49 eV *vs.* NHE.

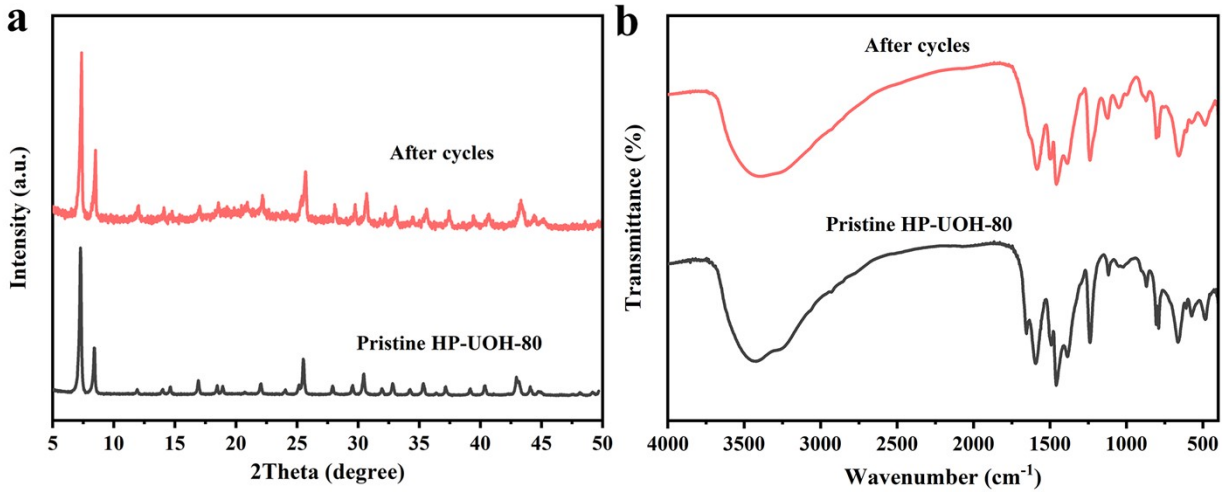

Fig. S10 (a) The PXRD patterns and (b) FTIR spectra of fresh HP-UOH-80 and used HP-UOH-80.

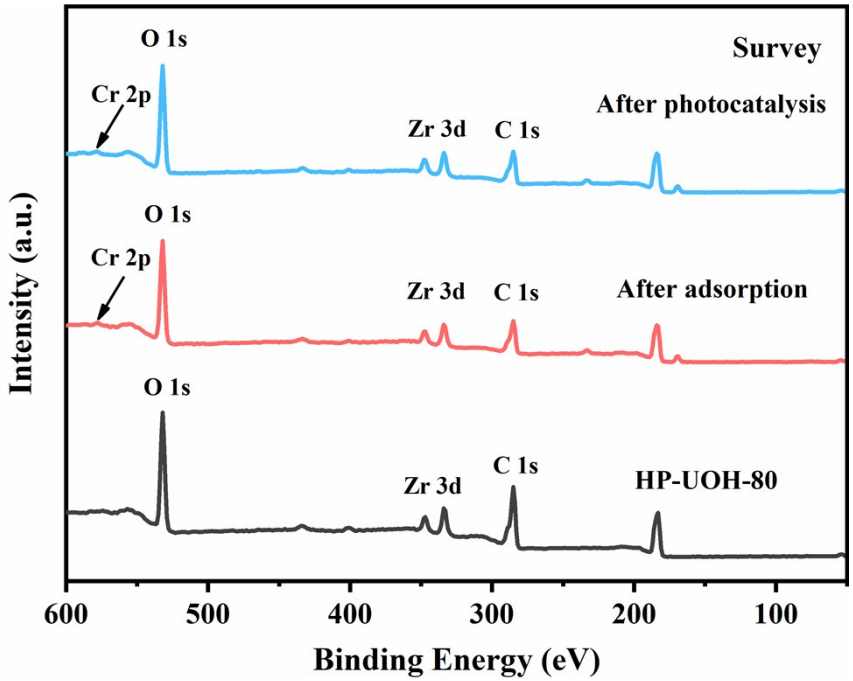

Fig. S11 The XPS survey scan of HP-UOH-80 and its corresponding after adsorption and photocatalysis.

References

[1] C. Zhao, J. Wang, X. Chen, Z. Wang, H. Ji, L. Chen, W. Liu, C.C. Wang, Bifunctional $Bi_{12}O_{17}Cl_2$/MIL-100(Fe) composites toward photocatalytic Cr(VI) sequestration and activation of persulfate for bisphenol A degradation, Sci. Total Environ. 752 (2021) 141901.